


Phonon-boundary scattering in nanoporous silicon films: Comparison of Monte Carlo techniques

Cite as: J. Appl. Phys. **122**, 125101 (2017); <https://doi.org/10.1063/1.4993601>

Submitted: 29 June 2017 . Accepted: 04 September 2017 . Published Online: 22 September 2017

Kevin D. Parrish, Justin R. Abel, Ankit Jain, Jonathan A. Malen, and Alan J. H. McGaughey 



View Online



Export Citation



CrossMark

ARTICLES YOU MAY BE INTERESTED IN

Nanoscale thermal transport

Journal of Applied Physics **93**, 793 (2003); <https://doi.org/10.1063/1.1524305>

Nanoscale thermal transport. II. 2003–2012

Applied Physics Reviews **1**, 011305 (2014); <https://doi.org/10.1063/1.4832615>

Effective phonon mean free path in polycrystalline nanostructures

Applied Physics Letters **106**, 171901 (2015); <https://doi.org/10.1063/1.4918703>

Applied Physics Reviews
Now accepting original research

2017 Journal
Impact Factor:
12.894

Phonon-boundary scattering in nanoporous silicon films: Comparison of Monte Carlo techniques

Kevin D. Parrish, Justin R. Abel, Ankit Jain, Jonathan A. Malen,
and Alan J. H. McGaughey^{a)}

Department of Mechanical Engineering, Carnegie Mellon University, Pittsburgh, Pennsylvania 15213, USA

(Received 29 June 2017; accepted 4 September 2017; published online 22 September 2017)

The thermal conductivities of silicon thin films with periodic pore arrays (i.e., nanoporous films) and square silicon nanowires are predicted at a temperature of 300 K. The bulk phonon properties are obtained from lattice dynamics calculations driven by first-principles calculations. Phonon-boundary scattering is included by applying three Monte Carlo-based techniques that treat phonons as particles. The first is a path sampling technique that modifies the intrinsic bulk mean free paths without using the Matthiessen rule. The second uses ray-tracing under an isotropic assumption to calculate a single, mode-independent boundary scattering mean free path that is combined with the intrinsic bulk mean free paths using the Matthiessen rule. The third modifies the ray-tracing technique to calculate the boundary scattering mean free path on a modal basis. For the square nanowire modeled using isotropic ray-tracing, the maximum mean free path is comparable to the wire width, an unphysical result that is a consequence of the isotropic approximation. Free path sampling and modal ray-tracing produce physically meaningful mean free path distributions. The nanoporous film thermal conductivity predictions match a previously measured trend, suggesting that coherent effects are not relevant to thermal transport at room temperature. A line-of-sight for phonons in the nanoporous films is found to change how thermal conductivity scales with porosity.

Published by AIP Publishing. [<http://dx.doi.org/10.1063/1.4993601>]

I. INTRODUCTION

As the porosity of a solid increases, its effective thermal conductivity decreases. The decreased cross-sectional area and the increased tortuosity that the heat flux must follow can be accounted for by solving the heat diffusion equation using the bulk (i.e., intrinsic) thermal conductivity. We will refer to the ratio between the solved effective thermal conductivity and the input intrinsic thermal conductivity as the continuum correction factor. When the feature sizes of the porous material are on the order of the fundamental energy carriers' mean free paths, boundary scattering of these carriers results in a reduction of the intrinsic thermal conductivity in addition to the continuum effect.

A porous material that exhibits both thermal conductivity reduction mechanisms is a silicon film of thickness tens to hundreds of nanometers that has a periodic two-dimensional array of pores of radii tens to hundreds of nanometers that span the film thickness.^{1–18} We will refer to such structures as nanoporous films. Due to silicon amorphization at the pore edges during fabrication and the formation of an amorphous native oxide layer when exposed to air, nanoporous films are not truly periodic from an atomistic standpoint.¹¹ The thin film boundaries and pore walls both scatter phonons, which are the dominant thermal energy carriers in silicon. The thermally relevant bulk phonon mean free paths span five orders of magnitude at room temperature, from 1 nm to 100 μm , and the wavelengths of the thermally relevant phonons are 1 to 5 nm.¹⁹ The nanostructuring reduces the in-plane thermal

conductivity to 1%–70% of the bulk value at room temperature.^{1,4,20} The suppression of the phonon thermal conductivity makes nanoporous silicon films attractive as a possible thermoelectric material.^{2,21} These structures provide a large parameter space to explore in terms of the pore lattice design, pore size, and pore spacing.

To further understand and ultimately predict the experimentally measured reduction in thermal conductivity, nanoporous silicon films have also been modeled computationally. When the structure is small enough [i.e., feature sizes $\mathcal{O}(1\text{ nm})$], the dynamics can be modeled atomistically and the thermal conductivity can be predicted from molecular dynamics simulations.^{21–23} For thicker films and when the pore feature sizes are on the order of tens of nanometers or larger, solving the atomistic dynamics explicitly is not possible due to computational limitations. Mesoscale approaches that modify the bulk phonon properties based on the nanostructure geometry are required.^{20,24–34} The effect of the boundary scattering on phonon transport and thermal conductivity can be determined by (i) spatially and temporally solving the Boltzmann transport equation in the geometry of interest^{20,25–31} or (ii) directly modifying the phonon mean free paths, as we explore herein.

Controversy exists as to whether or not wave-like (also referred to as coherent) phonon effects contribute to thermal transport in nanoporous silicon films at room temperature (i.e., are phonon modes related to the secondary periodicity introduced by the pores relevant?). Such effects have been observed at cryogenic temperatures, where the dominant phonon wavelengths are similar to the feature sizes.^{6,35–38} Jain *et al.*²⁴ modeled nanoporous silicon films with feature

^{a)}Electronic mail: mcgaughey@cmu.edu

sizes greater than 100 nm using the free path sampling technique and compared their in-plane thermal conductivity predictions to the experimental measurements of El-Kady *et al.*⁴ at a temperature of 300 K. They reproduced the fine structure of the experimental values without the inclusion of coherent effects. Alaie *et al.* experimentally measured the in-plane thermal conductivity of nanoporous silicon films with a minimum feature size of 250 nm at room temperature.¹¹ Through comparison to analytical models, they concluded that the thermal conductivity had a contribution from coherent phonon modes. Lee *et al.* measured the in-plane thermal conductivity of nanoporous silicon films with periodic and aperiodic pores.¹⁸ Their thermal conductivity predictions from ray-tracing calculations agree with the measurements on both the periodic and aperiodic structures within the experimental uncertainty. They concluded that coherent effects are not important at room temperature in nanoporous silicon films with feature sizes of 100 nm or larger.

The importance of pathways for ballistic phonon transport, i.e., line-of-sight, in silicon nanoporous films has also been investigated. Using a Boltzmann transport equation-based approach, Tang *et al.* found that staggering square pores in a film reduces the thermal conductivity compared to aligned pores.²⁰ Experimentally, Anufriev *et al.* measured a difference in the thermal conductivity of silicon structures of the same porosity with simple cubic (SC) and staggered pores.³⁸ They attributed a lower thermal conductivity in the staggered geometry to the boundary scattering of ballistic phonons.

The objective of this study is to compare thermal conductivity predictions for square silicon nanowires and nanoporous silicon films inspired by the structures of Alaie *et al.*¹¹ from three Monte Carlo-based techniques for modeling phonon-boundary scattering: (i) the free path sampling technique of McGaughey and Jain,³⁹ (ii) the isotropic ray-tracing technique of Hori *et al.*,⁴⁰ and (iii) a modal ray-tracing technique that we introduce. The nanoporous structures are described in Sec. II A, and the bulk phonon calculations are detailed in Sec. II B. The Monte Carlo techniques are presented in Secs. II C–II F and compared in terms of their underlying assumptions and computational requirements. The predictions are presented and analyzed in Sec. III, where we find no evidence for the existence of coherent phonon effects in the structures of Alaie *et al.* For the nanoporous films, we investigate how limiting the line-of-sight of phonons influences thermal conductivity.

II. METHODOLOGY

A. Nanoporous structures

The five nanoporous silicon films to be studied are based on the fabricated samples of Alaie *et al.*¹¹ and are shown in

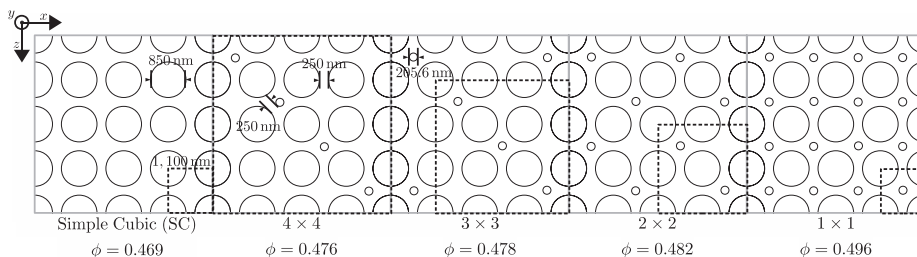


Fig. 1. The film thickness is 366 nm, and the pores completely penetrate the film. The large pores are present in all five structures. They have a radius of 425 nm and a periodicity of 1100 nm such that the edge-to-edge distance between them is 250 nm. Interpenetrating small pores are introduced with varying periodicity leading to the 1×1 , 2×2 , 3×3 , and 4×4 structures. The structure without any interpenetrating small pores will be referred to as SC structure. The small pore radius of 102.8 nm is chosen so that the distance from its edge to the nearest large pore edge is 250 nm (i.e., the minimum feature size is the same in all five structures). The resulting, Φ , porosities range from 0.469 to 0.496.

B. Bulk phonon calculation

The thermal conductivity in the Cartesian direction α , k_α , is calculated from

$$k_\alpha = \sum_\nu \sum_{\mathbf{q}} c_{\text{ph}}(\mathbf{q}, \nu) v_{\mathbf{g},\alpha}^2(\mathbf{q}, \nu) \frac{\Lambda(\mathbf{q}, \nu)}{|\mathbf{v}_{\mathbf{g}}(\mathbf{q}, \nu)|}, \quad (1)$$

where ν is the polarization, \mathbf{q} is the wavevector, c_{ph} is the phonon volumetric heat capacity, $\mathbf{v}_{\mathbf{g}}$ is the group velocity vector, and Λ is the mean free path.

To predict the thermal conductivity of the silicon nanostructures, we use the bulk phonon properties with the mean free paths modified with a boundary scattering model (Secs. II C–II F). In making this choice, we are assuming that: (i) there are no confinement effects (i.e., there are no bulk wavelengths that cannot exist in the nanostructure), as the wavelengths of thermally relevant phonons in silicon at room temperature (1–5 nm)¹⁹ are much smaller than the minimum feature size and (ii) phonon modes that exist based on the second periodicity of the nanoporous film (i.e., coherent modes) do not contribute to thermal transport. Subsequently, our calculations follow a particle-based transport description where Eq. (1) is valid.

The phonon frequencies, which provide the volumetric heat capacity (from Bose-Einstein statistics) and the group velocity vector, and bulk mean free paths are obtained using lattice dynamics calculations for bulk silicon at a temperature of 300 K.^{19,41–44} The required force constants were calculated using the density functional theory package Quantum ESPRESSO,⁴⁵ with an electronic wavevector grid of $8 \times 8 \times 8$ and an energy cutoff of 60 Ry on the primitive (i.e., two-atom) unit cell. We used the local density approximation exchange-correlation with the norm-conserving pseudopotential Si.pz-vbc.UPF. The harmonic force constants were obtained through density functional perturbation theory calculations using a phonon wavevector grid of $8 \times 8 \times 8$,

FIG. 1. Schematic diagrams of the top views of the five nanoporous films. The minimum repeating cell is outlined using a dashed line. The structures are periodic in the x - and z -directions.

which was interpolated to a $24 \times 24 \times 24$ wavevector grid resulting in 82944 phonon modes. The cubic force constants were calculated from finite displacements of a 216-atom supercell. The predicted bulk silicon thermal conductivity is 152 W/m K,⁴⁶ which is converged to within 2% for the chosen parameter set.⁴⁷ This value agrees with the experimentally measured thermal conductivity for isotopically pure silicon of 153 ± 5 W/m K.⁴⁸ As discussed by Jain and McGaughey, we note that the choice of exchange-correlation and pseudopotential can change the thermal conductivity value by up to 21 W/m K for the same convergence parameters.⁴⁷ We ignore phonon-isotope scattering as it can obscure the boundary scattering effects. Isotopically pure silicon has a 10% higher thermal conductivity than natural silicon.⁴⁸ The continuum correction factor for each geometry was calculated using COMSOL Multiphysics[®] to solve the heat diffusion equation using the finite element method.

C. Free path sampling

The free path sampling technique takes pre-calculated bulk phonon properties, specifically the group velocity vector and the intrinsic mean free path, and calculates the effective mean free path based on the geometry of the structure.³⁹ For each phonon mode with intrinsic mean free path $\Lambda_{pp}(\mathbf{q}, \nu)$, a number of free paths are sampled from a Poisson distribution. Each phonon is started from a random position inside the structure. In the periodic structures modeled here, the initial position is taken in the minimum repeating cell. The phonon is then traced from its origin in the direction of its group velocity vector until it either reaches the end of its free path or it encounters a boundary. If the phonon encounters a boundary, its free path is truncated as the distance from the origin to the boundary; otherwise, the free path remains the same. After all the free paths are found, they are averaged to provide the effective mean free path $\Lambda(\mathbf{q}, \nu)$, which contains information from both the intrinsic scattering and the geometry-specific boundary scattering. The thermal conductivity is then calculated from Eq. (1) using the new effective mean free paths.

Free path sampling directly modifies the intrinsic mean free paths based on the phonon-boundary scattering to calculate the effective mean free paths. This formulation is in contrast to the ray-tracing techniques, where the scattering rates are calculated separately and then combined using the Matthiessen rule. In this way, free path sampling avoids the assumption of independence of the scattering rates as changes to the intrinsic mean free path change the boundary scattering rate and vice versa.

D. Isotropic ray-tracing

The isotropic ray-tracing technique developed by Hori *et al.* calculates a single boundary scattering mean free path for all modes, $\bar{\Lambda}_{bdy}$, based on ballistic transmission (i.e., in the absence of intrinsic scattering).⁴⁰ The thermal conductance contribution, G , of a ballistic phonon mode in an isotropic system of length L is⁴⁹

$$G = \frac{1}{3} \frac{c_{ph}}{L} |\mathbf{v}_g| \bar{\Lambda}_{bdy}. \quad (2)$$

The thermal conductance of this mode can also be defined from an isotropic Landauer formalism as⁴⁹

$$G = \frac{1}{2} c_{ph} |\mathbf{v}_g| \int_0^{\pi/2} \mathcal{T}(\theta) \cos \theta \sin \theta d\theta, \quad (3)$$

where θ is the zenith angle off the normal of the plane at the beginning of the nanostructure and $\mathcal{T}(\theta)$ is the transmission probability through the nanostructure. From Eqs. (2) and (3)

$$\bar{\Lambda}_{bdy} = \frac{3}{2} L \int_0^{\pi/2} \mathcal{T}(\theta) \cos \theta \sin \theta d\theta. \quad (4)$$

The initial position of the ray-trace is sampled uniformly across the beginning plane of the nanostructure (i.e., the xy -plane when energy transmission is in the z -direction, see Fig. 1). The initial azimuthal angle is uniformly sampled from $[0, 2\pi]$ while the zenith angle is integrated from $[0, \pi/2]$ in 90 evenly sized increments. When the ray-trace encounters a boundary (e.g., a pore wall or the film boundary), it scatters diffusely in accordance with the Lambert cosine law. The ray-tracing terminates when the phonon either encounters the end of the structure (a transmission event) or when it returns to the beginning of the structure (a reflection event). The ratio of rays encountering the end of the structure to the total number of rays is the transmission ratio, $\mathcal{T}(\theta)$. Here, the transmission ratio is calculated by randomly sampling the initial x -position, y -position, and azimuthal angle. To model an infinite structure, as we do here, the structure length is increased until $\bar{\Lambda}_{bdy}$ is converged. Isotropic ray-tracing is equivalent to the Casimir limit.⁴⁰ No knowledge of the intrinsic phonon properties is required; it only depends on geometry.

The Matthiessen rule is then used to determine the mean free path of each phonon mode in the nanostructure as^{43,50,51}

$$\frac{1}{\Lambda(\mathbf{q}, \nu)} = \frac{1}{\Lambda_{pp}(\mathbf{q}, \nu)} + \frac{1}{\bar{\Lambda}_{bdy}}. \quad (5)$$

The Matthiessen rule assumes scattering mechanisms to be independent. Its applicability to phonon-boundary and phonon-isotope scattering has recently been investigated. Luisier found that the Matthiessen rule overestimated the thermal conductivity of roughened silicon nanowires due to an additional scattering contribution of localized surface modes coupled to phonon-phonon scattering.⁵² Similarly, Feng *et al.* reported an overestimation of thermal conductivity calculated by the Matthiessen rule in bulk silicon that resulted from a failure to account for coupling between impurity and phonon-phonon scattering.⁵³

E. Modal ray-tracing

The ray-tracing formulation of Hori *et al.* assumes that the phonon dispersion is isotropic and ignores modal details. To investigate the difference between free path sampling and isotropic ray-tracing, we introduce a formalism of the ray-tracing technique where the boundary scattering mean

free path is obtained on a modal basis. This approach allows us to eliminate the isotropic approximation in the ray-tracing calculation but not the use of the Matthiessen rule. We start the ray-trace by initializing the angle off the initial plane from the group velocity vector of a specific phonon mode. The calculation then traces the ray as it diffusely scatters with boundaries according to the Lambert cosine distribution as with isotropic ray-tracing. A mode-specific transmission ratio, $\mathcal{T}(\mathbf{q}, \nu)$, is then calculated.

As derived in the [Appendix](#), the mode-specific boundary mean free path $\Lambda_{\text{bdy}}(\mathbf{q}, \nu)$ is

$$\Lambda_{\text{bdy}}(\mathbf{q}, \nu) = \frac{L|\mathbf{v}_g(\mathbf{q}, \nu)|}{v_z(\mathbf{q}, \nu)} \mathcal{T}(\mathbf{q}, \nu). \quad (6)$$

The effective mean free path is then found by the Matthiessen rule from

$$\frac{1}{\Lambda(\mathbf{q}, \nu)} = \frac{1}{\Lambda_{\text{pp}}(\mathbf{q}, \nu)} + \frac{1}{\Lambda_{\text{bdy}}(\mathbf{q}, \nu)}. \quad (7)$$

To save computational time, only phonon modes that have $v_z > 0$ need to be considered for systems that are symmetrical about the z -direction. Phonon modes with $v_z < 0$ have the same $\Lambda_{\text{bdy}}(\mathbf{q}, \nu)$ as their positive counterpart in the evaluation of Eq. (1). The number of modes that must be ray-traced can be further reduced by taking advantage of other symmetries. Phonon modes with $v_z = 0$ make no contribution to the flux in that direction and have a boundary scattering mean free path of zero.

F. Convergence and comparison

The square nanowire is finite in the x - and y -directions and is infinite in the z -direction. For free path sampling, it is modeled by applying periodic boundary conditions in the z -direction. The free path sampling calculations were performed with 100000 samples of each phonon mode. The calculation was run with ten different initial seeds, and the 95% confidence interval on the predicted thermal conductivity is less than 0.1 W/m K. To approximate an infinite structure for the isotropic and modal ray-tracing calculations, the length must be increased until the predicted thermal conductivity is converged to a set tolerance. For all wire side lengths considered, we performed isotropic ray-tracing calculations with a length of 1 mm in the z -direction with 100000 samples of each zenith angle and initial position. The calculation was run with ten different initial seeds, and the 95% confidence interval is less than 0.5 W/m K. Increasing the length to 10 mm led to a difference in thermal conductivity of less than 2 W/m K. Modal ray-tracing calculations with a length of 1 mm in the z -direction were performed with 100000 samples of each phonon mode. The calculation was run with ten different initial seeds, and the 95% confidence interval is less than 0.5 W/m K. Increasing the length to 10 mm led to a difference in the thermal conductivity of less than 2 W/m K.

The minimum repeating structures for the each of the nanoporous silicon films are outlined by dashed lines in Fig. 1. For the free path sampling calculations, this structure is chosen and periodic boundary conditions are applied in the in-plane

(x - and z -) directions. The free path sampling calculations were performed with 100000 samples of each phonon mode. The calculation was run with ten different initial seeds, and the 95% confidence interval on the predicted thermal conductivity is less than 0.1 W/m K. Isotropic ray-tracing calculations with 50 cell repetitions in the z -direction were performed with 100000 samples of each zenith angle and initial position. The calculation was run with ten different initial seeds, and the 95% confidence interval is less than 0.1 W/m K. Increasing the number of cells by ten led to a difference in thermal conductivity of less than 0.2 W/m K. Modal ray-tracing calculations with a length of 50 cell repetitions in the z -direction were performed with 100000 samples of each phonon mode. The calculation was run with ten different initial seeds, and the 95% confidence interval is less than 0.1 W/m K. Increasing the number of cells by ten led to a difference in the thermal conductivity of less than 0.1 W/m K.

A comparison of the three techniques is provided in Table I. For the specified phonon grid and convergence parameters, free path sampling is the most computationally efficient for our chosen material and structures. Isotropic ray-tracing and modal ray-tracing require 5 and 2750 times more computational effort. It is important to note that the computational cost for free path sampling and modal ray-tracing scales linearly with the number of modes, while that for isotropic ray-tracing is constant because it is mode-independent. The computational cost for modal ray-tracing could be reduced by calculating transmission ratios for a grid of azimuthal and zenith angles and then interpolating the transmission ratio for a specific phonon mode based on the direction of its group velocity vector.

Isotropic ray-tracing is independent of material, and the $\bar{\Lambda}_{\text{bdy}}$ calculated for a geometry can be used for multiple materials. This single value, however, is applied to all phonon modes. In contrast, free path sampling and modal ray-tracing depend on both geometry and material. Separate calculations must thus be performed for every combination, but they provide a mode-dependent boundary scattering mean free path. The Matthiessen rule, applied in isotropic ray-tracing and modal ray-tracing, potentially limits these techniques by assuming that the phonon-boundary scattering rate is independent of the intrinsic phonon-phonon scattering.

III. RESULTS

A. Square nanowire

We begin by studying thermal transport in square silicon nanowires with side lengths a ranging from 100 to 1000 nm

TABLE I. Comparison of free path sampling, isotropic ray-tracing, and modal ray-tracing techniques for including phonon-boundary scattering in thermal conductivity prediction.

Technique	Normalized time	Material independent?	Mode dependent?	Matthiessen rule?
Free path sampling	1	No	Yes	No
Isotropic ray-tracing	5	Yes	No	Yes
Modal ray-tracing	2750	No	Yes	Yes

at a temperature of 300 K. The thermal conductivity predictions from free path sampling, isotropic ray-tracing, and modal ray-tracing are plotted in Fig. 2. Also plotted is the thermal conductivity calculated from the analytical Casimir limit ($\bar{\Lambda}_{\text{bdy}} = 1.12a$) and the bulk phonon mean free paths by use of Eqs. (1) and (5). Thermal conductivity increases by a factor of two with increasing side length for all three techniques, exhibiting a more rapid change for the smaller wires. Isotropic ray-tracing closely follows the Casimir limit prediction, as expected, and as previously shown by Hori *et al.*⁴⁰ The free path sampling and modal ray-tracing predictions are 6% to 40% higher than those from isotropic ray-tracing. We note that the Casimir limit is only strictly valid in the limit where other scattering mechanisms have a much longer length scale than the boundary scattering feature sizes. This condition is not met for all phonon modes in silicon at room temperature, where the bulk mean free paths are as short as 1 nm.

The thermal conductivity accumulation functions, k_{accum} , for the three Monte Carlo techniques for side lengths of 100 and 1000 nm are plotted in Fig. 3. These curves represent the cumulative contribution of phonon modes with increasing mean free path to thermal conductivity. At a side length of 100 nm, the isotropic ray-tracing accumulation function spans one order of magnitude of mean free paths and terminates at 100 nm. This maximum mean free path is two orders of magnitude smaller than that for free path sampling and modal ray-tracing, where phonons spanning three orders of magnitude contribute to thermal conductivity. Isotropic ray-tracing only calculates one boundary scattering mean free path and applies it to all the phonon modes regardless of their direction [Eq. (5)]. With the use of the Matthiessen rule, no phonon mode can have a larger mean free path than $\bar{\Lambda}_{\text{bdy}}$ and thereby all mean free paths must terminate by this value, leading to an unphysically small maximum mean free path. Free path sampling and modal ray-tracing, on the other hand, account for the boundary scattering at the modal level. The directionality captured in these two techniques allows for phonons traveling primarily axially to have little to no boundary scattering compared to modes traveling primarily in the plane of

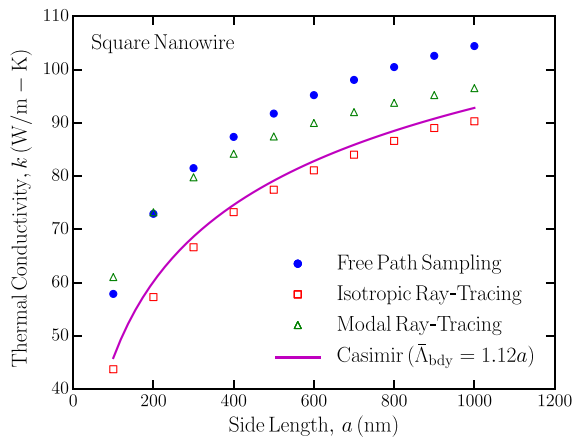


FIG. 2. Axial thermal conductivity of square silicon nanowires predicted by the three boundary scattering techniques and by the Casimir limit ($\bar{\Lambda}_{\text{bdy}} = 1.12a$). The 95% confidence interval is contained within the size of the markers.

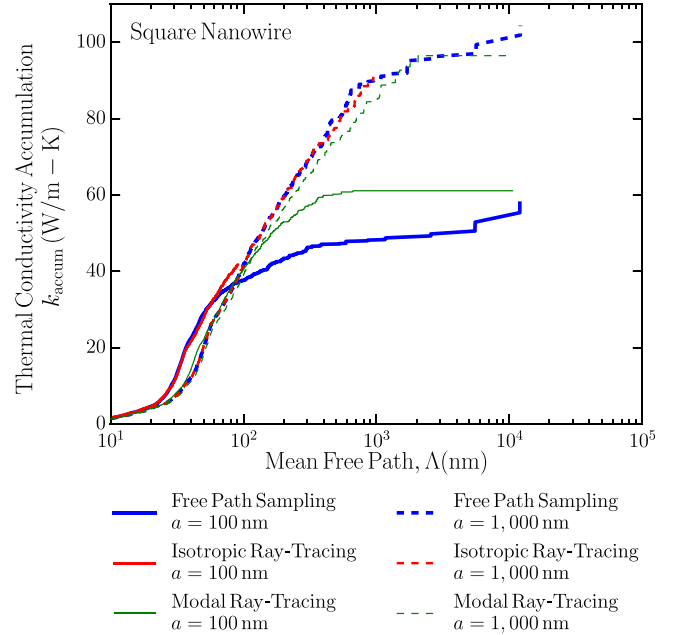


FIG. 3. Thermal conductivity accumulation of square silicon nanowires with side lengths of 100 and 1000 nm as predicted by the three boundary scattering techniques.

the wire. Because isotropic ray-tracing averages the boundary scattering in all directions, it fails to physically capture these long mean free path modes in the nanowire. Although free path sampling and modal ray-tracing produce similar thermal conductivities and accumulation functions, the predictions are not identical. The discrepancies could be a consequence of the use of the Matthiessen rule in modal ray-tracing.

When the side length is 1000 nm, the maximum mean free path for free path sampling and modal ray-tracing is one order of magnitude larger than that for isotropic ray-tracing. As the wire size is increased and the boundary scattering is decreased, the importance of including the directional dependence of boundary scattering is reduced. As the side length of the wire is further increased and the boundary scattering decreases, the predictions of all three techniques will converge to the bulk thermal conductivity and its accumulation function.

B. Nanoporous films

1. Thermal conductivity

We now investigate the nanoporous silicon films of Alaie *et al.* that were described in Sec. II A.¹¹ The in-plane thermal conductivities calculated by the three Monte Carlo techniques are plotted versus porosity in Fig. 4(a). These thermal conductivities include both the continuum correction factor and the effect of phonon-boundary scattering. The thermal conductivities are reduced by a factor of five compared to silicon's bulk thermal conductivity and decrease with increasing porosity. The thermal conductivity predictions from free path sampling and isotropic ray-tracing differ by less than 1 W/m K for each structure, a surprising agreement that was not found for the square nanowire. The modal ray-tracing values are 4–5 W/m K higher.

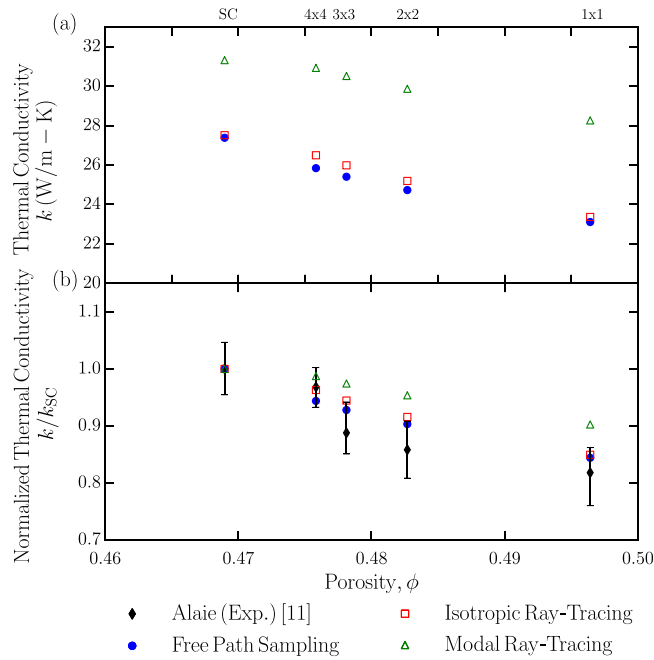


FIG. 4. (a) In-plane thermal conductivities of nanoporous silicon films from our calculations. (b) In-plane thermal conductivities normalized to the SC structure from the experiments by Alaie *et al.*¹¹ and from our calculations. The structures are identified in Fig. 1. The 95% confidence interval is contained within the size of the markers.

The thermal conductivity predictions are compared to the experimental measurements of Alaie *et al.* in Fig. 4(b).¹¹ Alaie *et al.* present thermal conductivities normalized by that of a solid thin film of the same thickness but do not provide the normalizing value. To compare our predictions to their measurements, we normalized the data in Fig. 4(a) to the SC structure. The Monte Carlo techniques all inherently treat phonons as particles such that they cannot capture coherent transport effects. All three techniques follow the experimental trend, with free path sampling lying within the experimental error bars for the four structures with interpenetrating small pores. This finding is consistent with the conclusions of Jain *et al.*²⁴ and Lee *et al.*,¹⁸ who found that particle-based models can predict the thermal conductivity of periodic silicon nanoporous films with feature sizes greater than 100 nm at room temperature.

2. Accumulation

The mean free path spectra produced by the Monte Carlo techniques are now compared by plotting the three thermal conductivity accumulation functions for the SC film in Fig. 5. The continuum correction factor is not included here so as to isolate the phonon-boundary scattering effect. The accumulations up to a mean free path of 300 nm are similar, with modal ray-tracing 4 W/m K below the other two techniques. Isotropic ray-tracing predicts a maximum mean free path that is an order of magnitude shorter than that from the other two techniques. As with the square nanowire, the origin of this difference is that phonon modes traveling in-plane encounter less scattering compared to modes traveling normal to the surfaces of the film. This geometrical effect is not captured by a single boundary scattering term. Because

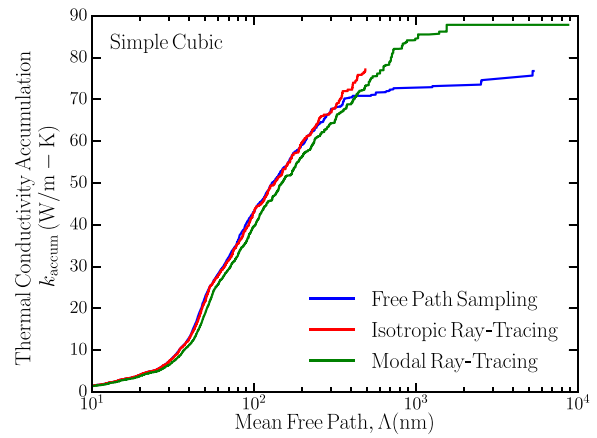


FIG. 5. Thermal conductivity accumulation of SC nanoporous silicon films in the in-plane direction from free path sampling, isotropic ray-tracing, and modal ray-tracing. The continuum correction factor is not applied.

of their modal nature, free path sampling and modal ray-tracing realize these long mean free paths.

3. Line-of-sight

We next examine the effect of line-of-sight, i.e., the distance a phonon can travel without boundary scattering. As noted in Sec. II F, free path sampling is less computationally expensive than the ray-tracing techniques. It is also more robust, as it does not require convergence with length, and captures directional effects as the scattering is calculated on a modal basis. We thus use free path sampling exclusively in the subsequent analysis.

The line-of-sight creates a limit on the largest free path in a nanoporous film, which can drastically change with a minimal change in porosity. Using the 1×1 structure from Fig. 1, we increase the radius of the interpenetrating small pore from 102.8 nm to 140 nm. At a radius of 102.8 nm, a phonon with a group velocity vector in the z -direction can propagate unimpeded between the large and small pores. At a small pore radius of 125 nm, corresponding to a porosity of $\phi = 0.5095$, the path becomes blocked as there is no line-of-sight from the current cell past the first nearest-neighbor cell. In Fig. 6, the

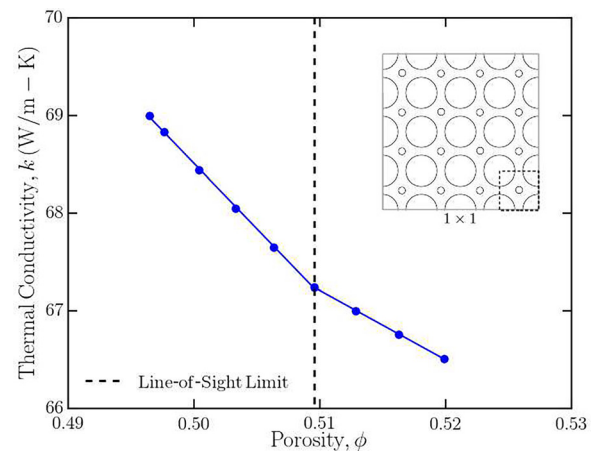


FIG. 6. Effect of interpenetrating pore radius on thermal conductivity for the 1×1 structure. The solid lines correspond to linear fits to the data on either side of the line-of-sight limit. The continuum correction factor is not applied.

intrinsic thermal conductivity of the 1×1 structure is plotted versus porosity. The continuum correction factor is not included here so as to isolate the phonon-boundary scattering effect. Lines fit to each side of the crossover radius of 125 nm show a 2.5% difference in slope that abruptly changes at the line-of-sight limit.

To further examine the line-of-sight effect, the distribution of free paths of the first longitudinal acoustic mode in the z -direction (wavevector of $7.164 \times 10^{-12} \text{ m}^{-1}$) for interpenetrating small pore radii of 120 and 130 nm is plotted in Figs. 7(a) and 7(b). For both structures, there is a steady decrease in the number of free paths from 200 to 1100 nm. This feature is from phonons that initialize between the small pores, with the rare limiting case that a phonon mode starts at the edge of one small pore and travels the full 1100 nm to the neighboring small pore. In the case of the 130 nm structure, this is the maximum distance a phonon can travel and limits the maximum free path. For a small pore size of 120 nm, the free paths extend more than two orders of magnitude past 1100 nm due to the gap between the large and small pores. It is the contribution of phonon modes that propagate through these gaps that changes the thermal conductivity scaling at a porosity of 0.5095, as shown in Fig. 6.

IV. SUMMARY

We applied three Monte Carlo-based techniques for including the effects of phonon-boundary scattering in predicting the thermal conductivities of silicon square nanowires (Fig. 2) and silicon nanoporous films (Fig. 4) at a temperature of 300 K. All three techniques treat the phonons as particles and thus do not include coherent effects.

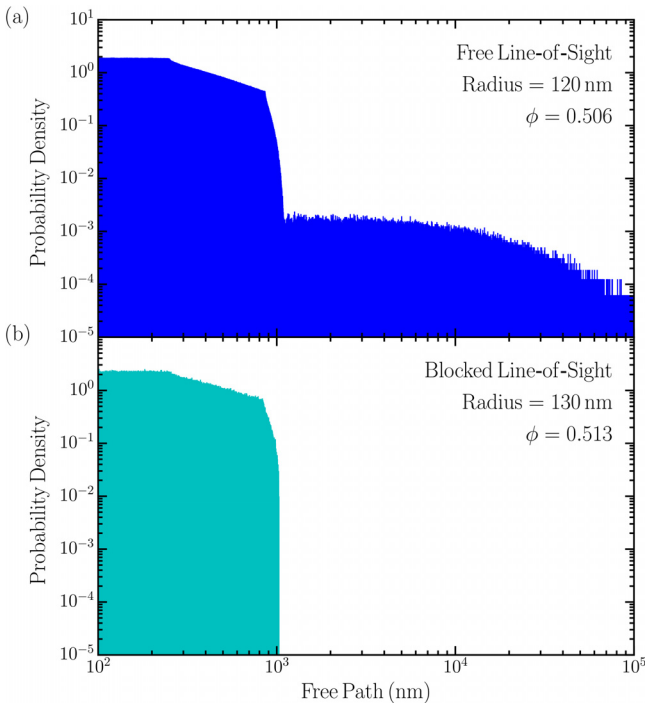


FIG. 7. Probability density of free paths of the first [001] longitudinal mode calculated from free path sampling for the 1×1 structure with interpenetrating small pores of radii (a) 120 nm and (b) 130 nm.

For the square nanowire, isotropic ray-tracing reproduced the Casimir limit while free path sampling and modal ray-tracing predicted larger thermal conductivities. The corresponding thermal conductivity accumulation functions show a large discrepancy in the range of maximum mean free paths. Isotropic ray-tracing predicts that only mean free paths up to the wire side length contribute to thermal conductivity, while the other two techniques predict the existence of mean free paths up to the bulk values. This difference is a result of isotropic ray-tracing's failure to account for differences in scattering due to directionality, while the other two techniques calculate the boundary scattering on a modal basis.

The thermal conductivity predictions for the nanoporous films from the three techniques fall within a range of 6 W/m K. Those from free path sampling agree with the measurements of Alaie *et al.*¹¹ within their respective uncertainties. This finding supports the conclusion obtained by others^{18,24} that coherent effects do not contribute to thermal transport at room temperature. Using free path sampling, we examined the effect of the line-of-sight by considering the 1×1 structure with an increasing porosity, as shown in Fig. 6. There is a distinct change in trend at the transition from a free line-of-sight to a blocked line-of-sight. This finding highlights the importance of line-of-sight in the engineering of thermal transport in nanostructures.

Although the three techniques for including phonon-boundary scattering produced similar thermal conductivity magnitudes and trends, there are distinct differences in the modal details. Isotropic ray-tracing reproduces the Casimir limit in the nanowire but truncates phonons that should not scatter with boundaries. This result emphasizes the limits of the applicability of the Casimir limit when applied to carriers with a broad spectrum of mean free paths. The formulation of modal ray-tracing, albeit at a higher computational cost, discriminates the boundary scattering of phonon modes based on their direction of propagation. Free path sampling has the advantages of operating on a modal basis, not invoking the Matthiessen rule, and having the lowest computational cost.

ACKNOWLEDGMENTS

We thank Takuma Hori and Junichiro Shiomi (the University of Tokyo) for useful discussions and insights. This work was supported by the CIT Bertucci fellowship, the CIT Bushnell fellowship, and NSF Award Nos. DMR-1507325 (AJHM) and ENG-1403447 (JAM).

APPENDIX: MODAL RAY-TRACING DERIVATION

The thermal conductance due to phonons traveling between two reservoirs with a small temperature difference is

$$G = \sum_{\nu} \left[\sum_{\mathbf{q}} \delta(v_z(\mathbf{q}, \nu) > 0) v_z(\mathbf{q}, \nu) \hbar \omega(\mathbf{q}, \nu) T(\mathbf{q}, \nu) \frac{df}{dT} \right] \Delta \mathbf{q}, \quad (\text{A1})$$

where δ is the Kronecker delta, f is the distribution function, T is the mean system temperature, and $\Delta \mathbf{q}$ is the volume in reciprocal space that modes of \mathbf{q} occupy.

Equation (A1) can be separated into the contribution from each mode, given by

$$G(\mathbf{q}, \nu) = v_z(\mathbf{q}, \nu) \hbar \omega(\mathbf{q}, \nu) \mathcal{T}(\mathbf{q}, \nu) \frac{df}{dT} \Delta \mathbf{q}. \quad (\text{A2})$$

In the ballistic transport regime, a mode's contribution to thermal conductance is

$$G(\mathbf{q}, \nu) = \frac{c_{\text{ph}} v_z^2(\mathbf{q}, \nu)}{L |\mathbf{v}_g(\mathbf{q}, \nu)|} \Lambda_{\text{bdy}}(\mathbf{q}, \nu). \quad (\text{A3})$$

Equating Eqs. (A2) and (A3) leads to

$$\Lambda_{\text{bdy}}(\mathbf{q}, \nu) = \frac{L |\mathbf{v}_g(\mathbf{q}, \nu)|}{v_z(\mathbf{q}, \nu)} \mathcal{T}(\mathbf{q}, \nu). \quad (\text{A4})$$

- ¹J.-K. Yu, S. Mitrovic, D. Tham, J. Varghese, and J. R. Heath, *Nat. Nanotechnol.* **5**, 718 (2010).
- ²J. Tang, H.-T. Wang, D. H. Lee, M. Fardy, Z. Huo, T. P. Russell, and P. Yang, *Nano Lett.* **10**, 4279 (2010).
- ³P. E. Hopkins, C. M. Reinke, M. F. Su, R. H. Olsson, E. A. Shaner, Z. C. Leseman, J. R. Serrano, L. M. Phinney, and I. El-Kady, *Nano Lett.* **11**, 107 (2011).
- ⁴I. F. El-Kady, R. H. Olsson, P. E. Hopkins, Z. C. Leseman, D. F. Goettler, K. Bongsang, C. M. Reinke, and M. F. Su, "Phonon manipulation with phononic crystals," *Technical Report No. SAND2012-0127* (Sandia National Laboratories, 2012).
- ⁵M. Nomura and J. Maire, *J. Electron. Mater.* **44**, 1426 (2014).
- ⁶N. Zen, T. A. Puurtinen, T. J. Isotalo, S. Chaudhuri, and I. J. Maasilta, *Nat. Commun.* **5**, 3435 (2014).
- ⁷M. Nomura, Y. Kage, J. Nakagawa, T. Hori, J. Maire, J. Shiomi, R. Anufriev, D. Moser, and O. Paul, *Phys. Rev. B* **91**, 205422 (2015).
- ⁸M. Nomura, J. Nakagawa, Y. Kage, J. Maire, D. Moser, and O. Paul, *Appl. Phys. Lett.* **106**, 143102 (2015).
- ⁹M. Nomura, Y. Kage, D. Miller, D. Moser, and O. Paul, *Appl. Phys. Lett.* **106**, 223106 (2015).
- ¹⁰J. Nakagawa, Y. Kage, T. Hori, J. Shiomi, and M. Nomura, *Appl. Phys. Lett.* **107**, 023104 (2015).
- ¹¹S. Alaie, D. F. Goettler, M. Su, Z. C. Leseman, C. M. Reinke, and I. El-Kady, *Nat. Commun.* **6**, 7228 (2015).
- ¹²R. Anufriev, J. Maire, and M. Nomura, *Phys. Rev. B* **93**, 045411 (2016).
- ¹³J. Lim, H.-T. Wang, J. Tang, S. C. Andrews, H. So, J. Lee, D. H. Lee, T. P. Russell, and P. Yang, *ACS Nano* **10**, 124 (2016).
- ¹⁴M. R. Wagner, B. Graczykowski, J. S. Reparaz, A. El Sachat, M. Sledzinska, F. Alzina, and C. M. Sotomayor Torres, *Nano Lett.* **16**, 5661 (2016).
- ¹⁵I. J. Maasilta, T. A. Puurtinen, Y. Tian, and Z. Geng, *J. Low Temp. Phys.* **184**, 211 (2016).
- ¹⁶T. A. Puurtinen and I. J. Maasilta, *Crystals* **6**, 72 (2016).
- ¹⁷T. A. Puurtinen and I. J. Maasilta, *AIP Adv.* **6**, 121902 (2016).
- ¹⁸J. Lee, W. Lee, G. Wehmeyer, S. Dhuey, D. L. Olynick, S. Cabrini, C. Dames, J. J. Urban, and P. Yang, *Nat. Commun.* **8**, 14054 (2017).
- ¹⁹K. Esfarjani, G. Chen, and H. T. Stokes, *Phys. Rev. B* **84**, 085204 (2011).
- ²⁰G. H. Tang, C. Bi, and B. Fu, *J. Appl. Phys.* **114**, 184302 (2013).
- ²¹J.-H. Lee, G. A. Galli, and J. C. Grossman, *Nano Lett.* **8**, 3750 (2008).
- ²²J.-H. Lee, J. C. Grossman, J. Reed, and G. Galli, *Appl. Phys. Lett.* **91**, 223110 (2007).
- ²³Y. He, D. Donadio, J.-H. Lee, J. C. Grossman, and G. Galli, *ACS Nano* **5**, 1839 (2011).
- ²⁴A. Jain, Y.-J. Yu, and A. J. H. McGaughey, *Phys. Rev. B* **87**, 195301 (2013).
- ²⁵S. Wolf, N. Neophytou, and H. Kosina, *J. Appl. Phys.* **115**, 204306 (2014).
- ²⁶N. K. Ravichandran and A. J. Minnich, *Phys. Rev. B* **89**, 205432 (2014).
- ²⁷T. Hori, G. Chen, and J. Shiomi, *Appl. Phys. Lett.* **104**, 021915 (2014).
- ²⁸B. Fu, G. H. Tang, and C. Bi, *J. Appl. Phys.* **116**, 124310 (2014).
- ²⁹G. Romano and J. C. Grossman, *J. Heat Transfer* **137**, 071302 (2015).
- ³⁰S. Wolf, N. Neophytou, Z. Stanojevic, and H. Kosina, *J. Electron. Mater.* **43**, 3870 (2014).
- ³¹G. Romano, K. Esfarjani, D. A. Strubbe, D. Broido, and A. M. Kolpak, *Phys. Rev. B* **93**, 035408 (2016).
- ³²Q. Hao, Y. Xiao, and H. Zhao, *J. Appl. Phys.* **120**, 065101 (2016).
- ³³Q. Hao, Y. Xiao, and H. Zhao, *Appl. Therm. Eng.* **111**, 1409 (2017).
- ³⁴Y.-C. Hua and B.-Y. Cao, *Appl. Therm. Eng.* **111**, 1401 (2017).
- ³⁵B. C. Daly, N. C. R. Holme, T. Buma, C. Branciard, T. B. Norris, D. M. Tennant, J. A. Taylor, J. E. Bower, and S. Pau, *Appl. Phys. Lett.* **84**, 5180 (2004).
- ³⁶A. D. O'Connell, M. Hofheinz, M. Ansmann, R. C. Bialczak, M. Lenander, E. Lucero, M. Neeley, D. Sank, H. Wang, M. Weides, J. Wenner, J. M. Martinis, and A. N. Cleland, *Nature* **464**, 697 (2010).
- ³⁷H. Okamoto, A. Gourgout, C.-Y. Chang, K. Onomitsu, I. Mahboob, E. Y. Chang, and H. Yamaguchi, *Nat. Phys.* **9**, 480 (2013).
- ³⁸R. Anufriev, A. Ramiere, J. Maire, and M. Nomura, *Nat. Commun.* **8**, 15505 (2017).
- ³⁹A. J. H. McGaughey and A. Jain, *Appl. Phys. Lett.* **100**, 061911 (2012).
- ⁴⁰T. Hori, J. Shiomi, and C. Dames, *Appl. Phys. Lett.* **106**, 171901 (2015).
- ⁴¹D. C. Wallace, *Phys. Rev.* **152**, 247 (1966).
- ⁴²D. C. Wallace, *Thermodynamics of Crystals* (Cambridge University Press, Cambridge, UK, 1972).
- ⁴³M. Dove, *Introduction to Lattice Dynamics* (Cambridge, Cambridge, 1993).
- ⁴⁴D. A. Broido, M. Malorny, G. Birner, N. Mingo, and D. A. Stewart, *Appl. Phys. Lett.* **91**, 231922 (2007).
- ⁴⁵P. Giannozzi, S. Baroni, N. Bonini, M. Calandra, R. Car, C. Cavazzoni, D. Ceresoli, G. L. Chiarotti, M. Cococcioni, I. Dabo, A. D. Corso, S. d. Gironcoli, S. Fabris, G. Fratesi, R. Gebauer, U. Gerstmann, C. Gougoussis, A. Kokalj, M. Lazzeri, L. Martin-Samos, N. Marzari, F. Mauri, R. Mazzarello, S. Paolini, A. Pasquarello, L. Paulatto, C. Sbraccia, S. Scandolo, G. Sclauzero, A. P. Seitsonen, A. Smogunov, P. Umari, and R. M. Wentzcovitch, *J. Phys.: Condens. Matter* **21**, 395502 (2009).
- ⁴⁶Our predicted bulk thermal conductivity value of 152 W/m K is higher than that of 144 W/m K reported by Jain *et al.*⁴⁷ for the same exchange-correlation and pseudopotential. The difference is a result of the harmonic force constants, calculated here from ph.x 6.0, while Jain *et al.* used ph.x 5.0.2.
- ⁴⁷A. Jain and A. J. H. McGaughey, *Comput. Mater. Sci.* **110**, 115 (2015).
- ⁴⁸A. V. Inyushkin, A. N. Taldenkov, A. M. Gibin, A. V. Gusev, and H.-J. Pohl, *Phys. Status Solidi C* **1**, 2995 (2004).
- ⁴⁹G. Chen, *Nanoscale Energy Transport and Conversion: A Parallel Treatment of Electrons, Molecules, Phonons, and Photons*, 1st ed. (Oxford University Press, 2005).
- ⁵⁰A. Matthiessen and C. Vogt, *Philos. Trans. R. Soc. London* **154**, 167 (1864).
- ⁵¹In their supplemental information, Hori *et al.*⁴⁰ present a variation of isotropic ray-tracing in which the bulk mean free path is used to probabilistically scatter the ray-trace, thus avoiding the use of the Matthiessen rule. We see no justification for including phonon-phonon scattering (a diffusive event) in the Landauer formalism, which is based on a ballistic conductance. We thus only consider the original ray-tracing technique and employ the Matthiessen rule.
- ⁵²M. Luisier, *Appl. Phys. Lett.* **103**, 113103 (2013).
- ⁵³T. Feng, B. Qiu, and X. Ruan, *Phys. Rev. B* **92**, 235206 (2015).